**Supplementary references, text and figures**

# Prevalence of non-aromatic carbonaceous molecules in the inner regions of circumstellar envelopes

Lidia Martínez[1+], Gonzalo Santoro[1+], Pablo Merino[1,2+], Mario Accolla[1], Koen Lauwaet[3], Jesús Sobrado[4], Hassan Sabbah[5], Ramón J. Pelaez[6], Victor J. Herrero[6], Isabel Tanarro[6], Marcelino Agúndez[2], Alberto Martín-Jimenez[3], Roberto Otero[3], Gary J. Ellis[7], Christine Joblin[5]*, José Cernicharo[2]* and José A. Martín-Gago[1]*

[1]Instituto de Ciencia de Materiales de Madrid (ICMM-CSIC). Materials Science Factory. Structure of Nanoscopic Systems Group. C/ Sor Juana Inés de la Cruz 3, 28049 Cantoblanco, Madrid, Spain.

[2]Instituto de Física Fundamental (IFF-CSIC). Group of Molecular Astrophysics, C/ Serrano 123, 28006 Madrid, Spain

[3]IMDEA Nanociencia, Ciudad Universitaria de Cantoblanco, 28049 Cantoblanco, Madrid, Spain

[4]Centro de Astrobiología (CAB, INTA-CSIC). Crta- de Torrejon a Ajalvir km4, 28850, Torrejon de Ardoz, Madrid, Spain.

[5]IRAP, Université de Toulouse, CNRS, CNES, 9 Av. du Colonel Roche, 31028 Toulouse Cedex 4, France

[6]Instituto de Estructura de la Materia (IEM-CSIC). Molecular Physics Department. C/Serrano 123, 28006 Madrid, Spain.

[7]Instituto de Ciencia y Tecnología de Polímeros (ICTP-CSIC). C/ Juan de la Cierva 3, 28006-Madrid, Spain.

[+] Equally contributed

*Corresponding authors: gago@icmm.csic.es, jose.cernicharo@csic.es, christine.joblin@irap.omp.eu

**Supplementary references**


1. Martínez, L. *et al.* Precisely controlled fabrication, manipulation and in-situ analysis of Cu based nanoparticles. *Sci. Rep.* **8,** 7250 (2018).
2. Kroto, H. W., Heath, J. R., O'Brien, S. C., Curl, R. F. & Smalley, R. E. C60 : Buckminsterfullerene. *Nature* **318,** 162–163 (1985).
3. Jäger, C., Mutschke, H., Henning, T. & Huisken, F. Spectral Properties of Gas-phase Condensed Fullerene-like Carbon Nanoparticles from Far-ultraviolet to Infrared Wavelengths. *Astrophys. J.* **689,** 249–259 (2008).
4. Carpentier, Y. *et al.* Nanostructuration of carbonaceous dust as seen through the positions of the 6.2 and 7.7 μ m AIBs . *Astron. Astrophys.* **548,** A40 (2012).
5. Jager, C. *et al.* Identification and Spectral Properties of Polycyclic Aromatic Hydrocarbons in Carbonaceous Soot Produced by Laser Pyrolysis. *Astrophys. J. Suppl. Ser.* **166,** 557–566 (2006).
6. Jäger, C., Huisken, F., Mutschke, H., Jansa, I. L. & Henning, T. Formation of polycyclic aromatic hydrocarbons and carbonaceous solids in gas-phase condensation experiments. *Astrophys. J.* **696,** 706–712 (2009).
7. Biennier, L. *et al.* Characterization of circumstellar carbonaceous dust analogues produced by pyrolysis of acetylene in a porous graphite reactor. *Carbon N. Y.* **47,** 3295–3305 (2009).
8. Kovačević, E., Stefanović, I., Berndt, J., Pendleton, Y. J. & Winter, J. A Candidate Analog for Carbonaceous Interstellar Dust: Formation by Reactive Plasma Polymerization. *Astrophys. J.* **623,** 242–251 (2005).
9. Contreras, C. S. & Salama, F. Laboratory investigations of polycyclic aromatic hydrocarbon formation and destruction in the circumstellar outflows of carbon stars. *Astrophys. Journal, Suppl. Ser.* **208,** (2013).
10. Maté, B., Molpeceres, G., Jiménez-Redondo, M., Tanarro, I. & Herrero, V. J. High-energy electron irradiation of interstellar carbonaceous dust analogs: cosmic-ray effects on the carriers of the 3.4 μ m absorption band . *Astrophys. J.* **831,** 51 (2016).
11. Agúndez, M. *et al.* Molecular abundances in the inner layers of IRC +10216. *Astron. Astrophys.* **543,** A48 (2012).
12. Fonfría, J. P. *et al.* The Abundance of C2H4in the Circumstellar Envelope of IRC+10216. *Astrophys. J.* **835,** 196 (2017).
13. Haberland, H. in *Gas-Phase Synthesis of Nanoparticles* (ed. Huttel, Y.) 3–21 (Wiley-VCH, 2017). doi:10.1002/9783527698417
14. Agúndez, M. *et al.* Growth of carbon chains in IRC +10216 mapped with ALMA⋆⋆⋆. *A&A* **601,** (2017).
15. Gail, H., & Sedlmayr, E. (2013). Physics and Chemistry of Circumstellar Dust Shells (Cambridge Astrophysics). Cambridge: Cambridge University Press. doi:10.1017/CBO9780511985607
16. Kousal, J. *et al.* Magnetron-sputtered copper nanoparticles: lost in gas aggregation and found by in situ X-ray scattering. *Nanoscale* **10,** 18275–18281 (2018).
17. Kwok, S. The synthesis of organic and inorganic compounds in evolved stars. *Nature* **430,** 985–991 (2004).
18. Kratochvíl, J., Kuzminova, A., Kylián, O. & Biederman, H. Comparison of magnetron sputtering and gas aggregation nanoparticle source used for fabrication of silver nanoparticle films. *Surf. Coatings Technol.* **275,** 296–302 (2015).

19. Haberland, H., Karrais, M. & Mall, M. A new type of cluster and cluster ion source. *Zeitschrift für Phys. D Atoms, Mol. Clust* **415,** 413–415 (1991).

20. Michau, A., Arnas, C., Lombardi, G., Bonnin, X. & Hassouni, K. Nanoparticle formation and dusty plasma effects in DC sputtering discharge with graphite cathode. *Plasma Sources Sci. Technol.* **25,** (2016).

21. De Toro, J. A., Normile, P. S. & Binns, C. in *Gas-Phase Synthesis of Nanoparticles* 39–55 (2017).

22. Binns, C. in *Handbook of Metal Physics* 49–71 (2009).

23. Selwyn, G. S., Weiss, C. A., Sequeda, F. & Huang, C. Particle contamination formation in magnetron sputtering processes. *J. Vac. Sci. Technol. A Vacuum, Surfaces, Film.* **15,** 2023–2028 (1997).

24. Sabbah, H. *et al.* Identification of PAH Isomeric Structure in Cosmic Dust Analogs: The AROMA Setup. *Astrophys. J.* **843,** 34 (2017).

25. Šedo, O., Alberti, M., Janča, J. & Havel, J. Laser desorption-ionization time of flight mass spectrometry of various carbon materials. *Carbon N. Y.* **44,** 840–847 (2006).

26. Horný, L., Petraco, N. D. K. & Schaefer, H. F. Odd carbon long linear chains HC2n+1H (n = 4-11): Properties of the neutrals and radical anions. *J. Am. Chem. Soc.* **124,** 14716–14720 (2002).

27. Maclagan, R. G. A. R. The proton affinity of C3H2. *J. Mol. Struct. THEOCHEM* **258,** 175–178 (1992).

28. Sánchez, J. P., Aguirre, N. F., Díaz-Tendero, S., Martín, F. & Alcamí, M. Structure, Ionization, and Fragmentation of Neutral and Positively Charged Hydrogenated Carbon Clusters: $C_n H_m^{q+}$ ( $n$ = 1–5, $m$ = 1–4, $q$ = 0–3). *J. Phys. Chem. A* **120,** 588–605 (2016).

29. Cordiner, M. A., Charnley, S. B., Kisiel, Z., McGuire, B. A. & Kuan, Y.-J. Deep K-band observations of TMC-1 with the Green Bank Telescope: Detection of HC7O, non-detection of HC11N, and a search for new organic molecules. *Astrophys. J.* **850,** 187 (2017).

30. McGuire, B. A. *et al.* Detection of Interstellar HC5O in TMC-1 with the Green Bank Telescope. *Astrophys. J.* **843,** L28 (2017).

31 A. Pinardi *et al*. Tailored formation of N-doped nanoarchitectures by diffusion-controlled on-surface (cyclo) dehydrogenation of heteroaromatics. ACS nano 7, 3676-3684 (2013)

## 1. The stardust machine and the CSE: Technical details.

### The Stardust machine for mimicking the CircumStellar Envelope (CSE)

The Stardust machine is a novel experimental setup designed to simulate in the laboratory the complex conditions of cosmic dust formation and processing in the environment of evolved stars or supernova. It comprises six interconnected ultra-high-vacuum (UHV) modules, offering a high level of control over both the fabrication and processing of cosmic dust analogues. In addition, a collection of *in situ* characterization techniques is available**.** In *Stardust* the chemistry proceeds via atom aggregation under conditions in which most of the reactions that occur are neutral-neutral, closely resembling what happens in the circumstellar envelopes (CSE) of Asymptotic Giant Branch (AGB) stars.

The *Stardust* machine was conceived as a multi-purpose experimental station. Thus, it has a versatile, modular design that allows easy reconfiguration of the machine based on the requirements of each specific experiment. Each module has been designed to simulate a given process in a given astrophysical environment. The first step corresponds to the generation of dust seeds, which can be produced at relatively low temperature in the first module, denominated *Multiple Ion Cluster Source (MICS)*, where atoms are ejected from up to three targets. During their transit along this module atoms start to aggregate through collisions with other ejected atoms and the growth process occurs. After production, the seeds pass through a *Diagnosis chamber*, where it is possible to monitor, filter and perform experiments on these pristinely formed seeds. Subsequently, the seeds enter the *Oven chamber*, a passageway where the seeds can be heated with IR radiation during their transit. This can provide temperatures similar to those found in the dust formation zone of AGBs. Upon exiting the *Oven chamber* the grains can be accelerated in the *Acceleration module*, in order to simulate radiation pressure or the escape of the grains towards the interstellar medium (ISM), where the material will cool down. Furthermore, gas phase molecules ($H_2$, $CH_4$, $C_2H_2$…) can be introduced into any of the previously described chambers in desired proportions, in order to promote gas-grain interactions.

After the fabrication of the dust analogues, the next modules are dedicated to both analysing the properties of the generated pristine analogues, as well as tackling the question of dust evolution in various astrophysical environments ranging from later stages of evolved stars (protoplanetary and planetary nebulae), to the ISM and protoplanetary disks. The *INFRA-ICE module* is dedicated to performing IR spectroscopy of analogues formed at variable temperature down to 12 K, allowing on-substrate (by collecting the analogues) dust processing and molecular ice growth. The final module is the *ANA* (Analysis Module) that consists of a UHV chamber in which the dust analogues are collected on a substrate and further analysed by a collection of surface science techniques (XPS, Auger, UPS, LEIS…). Here the collected analogues can be heated to up to 1200 K combined with various dust processing techniques. All the processes occurring to the dust analogues during heating, irradiation and exposure can be monitored *in situ* by the available characterization techniques**.**

A detailed technical description of the overall machine is provided in reference[1]. The experiments presented in this article correspond to a short configuration of the machine, in which only some of the modules have been used. Given the aforementioned need for highly controllable and clean environments to undertake proper laboratory simulations, only ultra-high vacuum (UHV) compatible materials and seals were used in the construction of the machine.

**Configuration of the Stardust set-up used in present experiments**

Although the modular concept of the Stardust machine allows to be mounted in different configurations, for this work only three chambers were employed: MICS, Acceleration and ANA. The MICS module is a sputter gas aggregation source (SGAS) devoted to nanoparticle (NP) and cluster fabrication. It incorporates lateral entrances in the aggregation zone through which both Optical Emission Spectroscopy (OES) and gas ($H_2$) injection is performed. The Acceleration module in this configuration is dedicated to monitor the NPs. In this work it was employed for sample collection for *ex situ* analysis and for Quadrupole Mass Spectrometry (QMS). Finally, the ANA module is devoted to *in situ* analysis of the NPs by electron spectroscopy techniques and thermal desorption spectroscopy. Further details of each module are given elsewhere[1]. Supplementary Figure 1 shows the configuration employed in this work. For the collection of the carbon star-dust analogues, two different fast entry points were used (in the Acceleration and ANA chambers). Unless otherwise specified, the samples were collected in the *Acceleration chamber*. The base pressure was $1x10^{-9}$ in MICS, $5x10^{-10}$ in Acceleration, and $1x10^{-10}$ mbar in ANA.

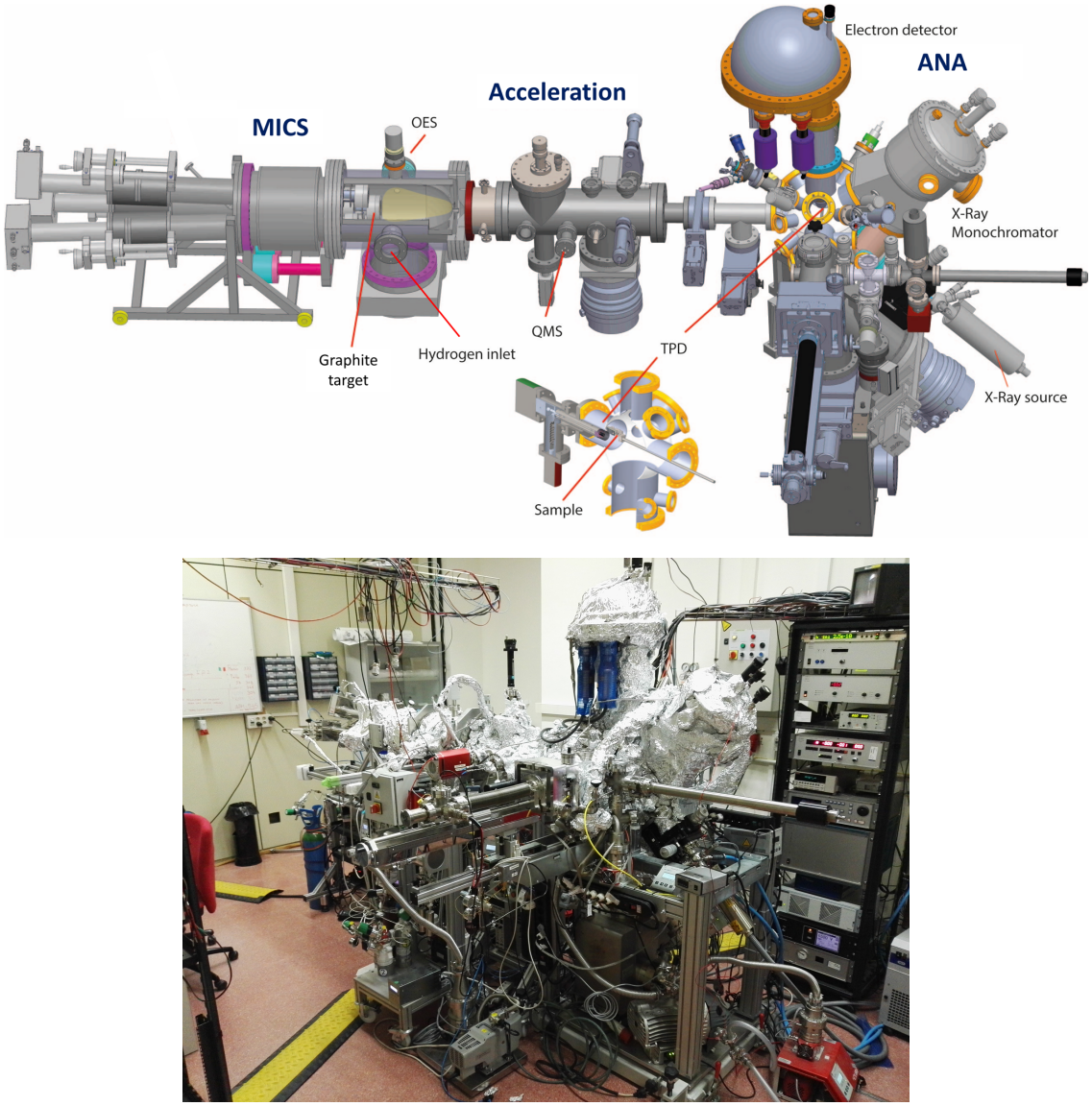


**Supplementary Figure 1**. Technical drawing (top) and photograph (bottom) of *Stardust* in the configuration employed for these experiments.

## 2.- Comparison between *Stardust* and other methods for fabricating carbon star-dust analogues.

Several methodologies for generating carbon star-dust analogues have been proposed in the literature resulting in a number of carbon products with different structure and hydrogen content. The main production techniques are summarized in Supplementary Table 1. This table collects the main physical parameters. Some of the parameters cannot be easily generalized as they are strongly dependent on the experimental conditions. This is the case of the total pressure, where a great deal of precision is needed to define this value (base pressure, pressure of the dragging or residual gas, partial pressure of the precursors, etc.). The list of references is representative and far from being exhaustive, as there are many of insightful experiments that have been performed in laboratory astrophysics.

***Supplementary table 1:*** *Comparison between typical techniques used to synthesize cosmic dust analogues.*

| Technique | Precursors | T (K) | Ion chemistry | Wall effect | Refs |
|---|---|---|---|---|---|
| Laser ablation | Graphite + quenching gas | ≥4000 | yes | no | [2,3] |
| Combustion/Flames | Hydrocarbons | 1800-2500 | weak | no | [4] |
| Pyrolysis (laser induced) | Hydrocarbons | 1000-1700 ≥3500 | no | depending on reactor | [5,6] |
| Pyrolysis | Hydrocarbons | 600-2000 | no | depending on reactor | [7] |
| Dusty plasmas | Hydrocarbons | 600-2000 | Weak/ strong | yes | [8–10] |
| SGAS: Sputter Gas aggregation sources: *Stardust* | Graphite + $H_2$ | <1000 | weak/no | no | This work |

All the aforementioned techniques have been used to describe different conditions and regions of the cosmos. However, they present limitations as the experiments used to mimic astrophysical environments need to be scaled to laboratory standards, and on many occasions, it is very difficult to validate a technical set-up as representative of particular astronomical conditions. This is mostly true when trying to reproduce the chemistry of the inner layers of CSE of evolved stars. In most of these experiments the chemistry involves high-energetic or ionic content, out of equilibrium processes, or relies on molecular precursors that must be decomposed. These conditions are far removed from those of the inner layers of CSE, where clustering takes place mostly by neutral-neutral reactions in the absence of other sources of radiation. In this respect, the *Stardust* machine was specifically conceived for reproducing the inner layers of the CSE, and its differential advantage with respect to the rest of the dust analogue production techniques is that the basic constituents from which the material grows are individual thermalized atoms. This is critical in all the three steps of the dust growth process and enables us to obtain chemical synthesis routes from reactions in equilibrium, as observed in C-rich AGB stars and some protoplanetary nebulae.

**Supplementary table 2.** *Table comparing the dust formation zone of CSEs with the experimental values used for experiments in Stardust.*

| Typical values in the dust formation zone of CSEs | Values at aggregation zone of *Stardust* | Comments |
|---|---|---|
| $n_{H2}=10^8$-$10^{12}$ $cm^{-3}$. Ref[11]<br>$n_{H2}/n_C = 10^3$ | $n_{H2}= 10^{10}$-$10^{12}$ $cm^{-3}$<br>$n_{H2}/n_C$ = 1-$10^2$ | *Stardust* densities are higher to accelerate the chemistry. The high end of the $H_2$/C ratio is close to that of the CSE. |
| Temperature range: 500-2000 K. Ref [11,12] | Temperature range: 300-500K | The chemical kinetics model suggests that the effect of temperature is critical for the formation of alkanes, which are favored at low temperatures. Close to the magnetron surface, temperature can reach around 1000K, although at the aggregation area could be bellow 500K.[13] |
| Absence of UV processing. Ref [14] | Absence of UV photons. | Possible UV photons from the UV interstellar field in low mass loss rate AGB stars or in very clumpy envelopes |
| Ionization degree: $<10^{-5}$. Ref[15] | Ionization degree: $10^{-5}$. Ref. [13] | The charge is found mainly on large particles after they are formed. Not playing important role in the chemistry of small molecules and clusters. |
| $n_{H2}/n_{c2H2}$: Estimated: $10^4$ Ref.[14] Detected: $10^7$ Ref. [16] | Acetylene is produced, not introduced : $n_{H2}/n_{C2H2}$: 50 | We produce an excess of $C_2H_2$ with respect to the star, however, still low enough to initiate cyclization in these conditions |
| Time in this area: 30 yr, to travel $10^{15}$ cm at a expansion velocoty of 10 km/s. · Ref [11] | Residence time in aggregation zones: seconds: Ref. [16] | In Stardust the Ar pressure close to the magnetron enables 3-body reactions |
| Gas phase aggregation from atoms | Gas phase aggregation from atoms | Not necessary to include molecular precursors to decompose as source of C or highly energetic plasma to initiate the chemistry |
| Shock waves. · Ref [17] | No shocks | Material formed in shocks cannot be simulated in *Stardust* |

**Sputter gas aggregation sources (SGAS) compared to Magnetron sputtering.** Gas phase condensation techniques have been widely reported as good candidates for the formation of cosmic dust grain analogues[6]. Traditionally, in gas aggregation sources (GAS) atoms are evaporated to a region containing a cooling working gas. Upon reaching supersaturation and due to the collisions with the cooling gas, the atoms may nucleate to nanoparticles. These nanoparticles are afterwards dragged through a nozzle into another chamber with lower pressure, usually employed for deposition of the nanoparticle beam on a substrate[18]. Haberland and co-workers[19] combined this idea of the GAS with magnetron sputtering and developed the so-called SGAS. The SGAS have some characteristics that clearly differentiate the technique from sputtering techniques commonly

used for the creation of dusty plasmas[20]. Biederman's group published a comparative study between both techniques[18]. One of the critical questions is the possibility of working at higher pressures of the working gas. Conventional sputtering processes usually operate in the $10^{-2}$ – $10^{-3}$ mbar range, while the pressure in the aggregation zone of a SGAS is in the range of 0.1-1 mbar[21]. In these conditions, clustering is highly efficient as the sputtered vapour is rich in dimers (formed by condensation of atoms and not directedly sputtered out from the targe), which helps to overcome the energy barriers involved in the first stages of cluster nucleation, as this is considered to be a critical bottleneck in the clustering process[22].

In SGAS, one chamber is used for sputtering and cluster growth and, subsequently, the nanoparticles are dragged by pressure difference into a secondary deposition chamber where the substrate is located. The SGAS process is not substrate dependent such that the nanoparticles, already formed in the first chamber, soft-land on the substrate instead of growing on the substrate as in conventional sputtering. Although the growth rates in SGAS are much slower than the sputtering processes (sputtering machines are designed to grow thick layers of a material on a substrate, whereas we focus on the first formed particles), the possibility to tune the size (typically 1-60 nm)[21] and the amount of nanoparticles generated with the variables of the process clearly represents and advantage in comparison to conventional sputtering, since lateral growth due to surface diffusion processes[23] is avoided.

Thus, in this article we propose the use of SGAS as a valuable and versatile technique for mimicking the conditions of CSE.

### 3. Atomic Force Microscope imaging (AFM).

AFM images were acquired *ex situ*, after fabrication of the samples using the fast entry point in the Acceleration chamber, marked as SAMPLE 1 position in Fig.1 of the main text. Supplementary Figure 2a corresponds to a deposition carried out during 10 min under the conditions described in the main text, whereby a nanoparticle rate of 8 NPs/$\mu m^2$·min can be derived. Most of the carbon is agglomerated in the form of nanometer size C-nanograins, as those that can be observed. Also, the substrate presents certain unresolved roughness comprised of smaller structures that may be related to the C/HC clusters detected with *AROMA* (white square in supplementary figure 2c). The features of the background and the C-nanograins can be easily differentiated from the line profiles. It is clear that on one hand there are C-nanograins of around 4 nm height (blue profile) and, even though they cannot be fully resolved using AFM, the structures depicted in the green profile present a height of around 1 nm. The former may be related to the structures presented in the STM analysis of Figure 2 in the main manuscript. The roughness of these small features is clearly larger than the roughness of the SiOx substrate (dashed-black line).

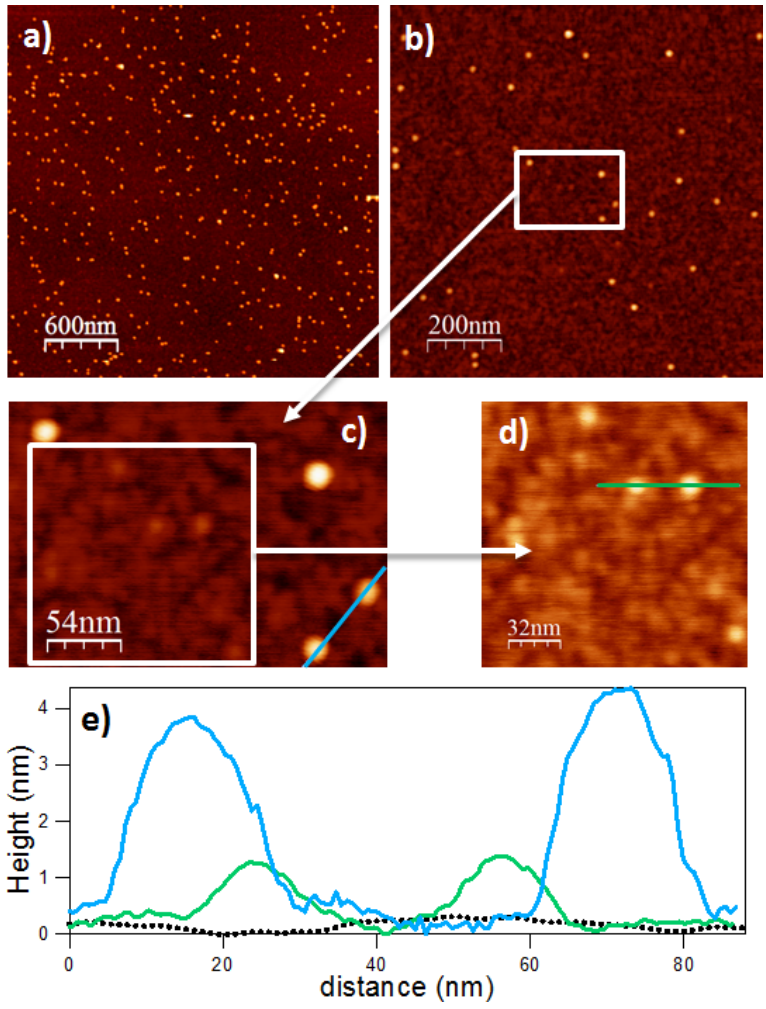


**Supplementary Figure 2.** AFM images of C-nanograins deposited on SiOx acquired at different magnifications. a) Image of 3 µm x 3 µm indicating the size homogeneity of the nanograins. b) Image of 1 µm x 1 µm of C-nanograins fabricated with half of the power employed for a) to have lower nanograin density and smaller features on the surface. c) Zoom of figure b). d) Zoom of figure c). e) Height Profiles obtained from the blue and green lines of c) and d), respectively, compared to the height profile in a SiOx substrate (dashed-black line). These images were recorded for a low hydrogen density.

## 4.- *In situ* optical emission spectroscopy

The emission spectra recorded during the production of carbon dust analogs in the aggregation zone of the stardust at different $H_2$ densities show that near infrared Ar lines prevailed in all cases, as shown in Supplementary Figure 3 for the 690 - 750 nm range. They correspond mainly to electronic transitions between the 4p-4s excited Ar levels, and extend up to 1000 nm. On the contrary, Ar emissions in the region 350-470 nm, corresponding to transitions 5p-4s that are usually very intense, have not been detected, due to the higher electron energy necessary to excite the upper level and to the fact that low Ar excitation temperatures (<1 eV) have been reported previously for this experimental system[1]. Furthermore, $C_2$ and CH could be detected with low $H_2$ densities (see insets in Supplementary Fig. 4 (a)), but these bands disappeared when a high $H_2$ density was added. At the same time, Ar intensities decreased noticeably with increasing $H_2$, while the ($H_\alpha$, $H_\beta$, $H\gamma$) atomic lines of the Balmer series appeared.

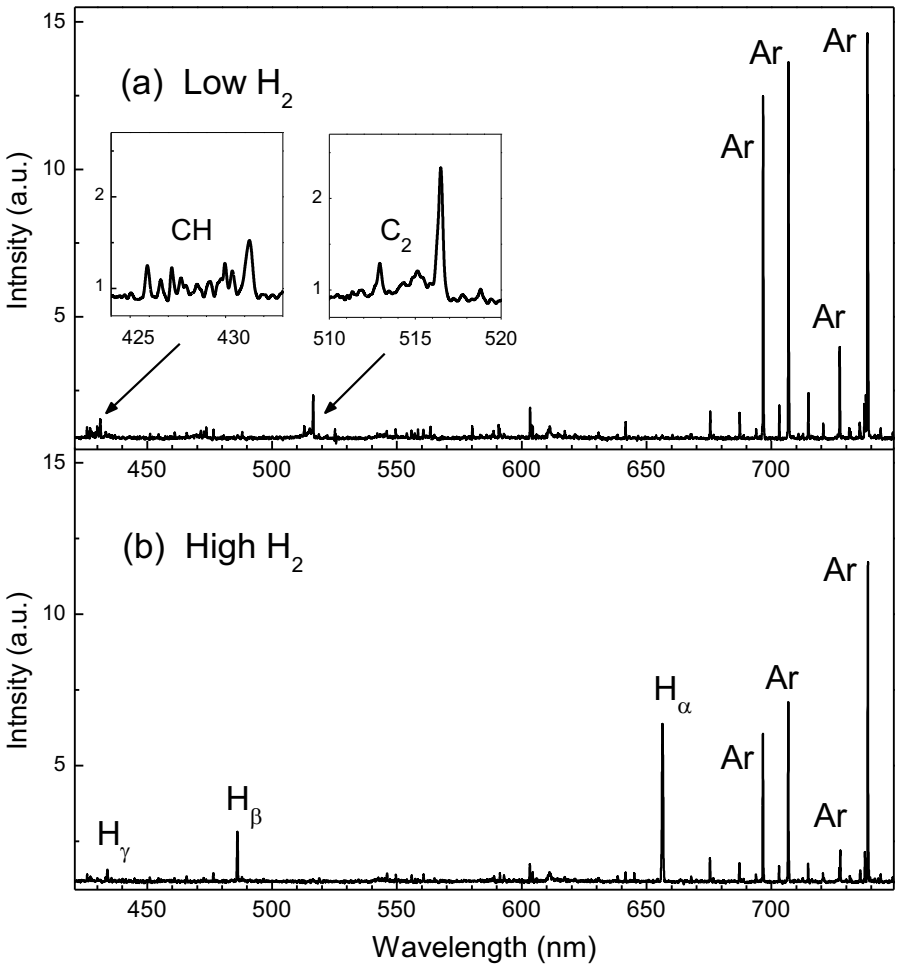


**Supplementary Figure 3. Optical emission spectrum of the plasma generated** in the aggregation zone of *Stardust* for a low (a) and a high (b) $H_2$ density. $H_2$ flow rates of $4x10^{-4}$ and 1 sccm were used, respectively.

## 5. Laser Desorption/Ionization (LDI) mass-spectrometry: the *AROMA* set-up

In order to obtain better insight into the molecular phase associated with the C-dust we have employed *ex situ* laser desorption ionization mass-spectrometry (LDI-MS) in the experimental set-up called *AROMA*[24]. The ion source offers the possibility of probing polycyclic aromatic hydrocarbons (PAHs), carbon clusters (C clusters), hydrogenated carbon clusters (HC clusters) and fullerenes in solid samples by performing by performing LDI in a single step[25] as well as using the laser desorption-laser ionization (L2MS) technique[24], in which desorption and ionization are separated in time and space and each step is performed with a different laser. In the L2MS scheme, the approach used in these experiments, an infrared laser pulse desorbs the solid material into the gas phase, with minimal fragmentation, and a subsequent ultraviolet (UV) laser pulse selectively ionizes the gas phase aromatic organic molecules. The ions generated are stored and thermalized in the linear quadrupole ion trap (LQIT) and then monitored with Time Of Flight (TOF) spectrosmetry. This technique has many advantages including its sensitivity. However, one drawback is that it is biased towards species that efficiently respond to the excitation scheme, in particular regarding ionization. For example, with the lasers used in our experiments, it is not possible to detect alkanes. On the other hand, the scheme is very sensitive to the detection of PAHs and fullerenes[24].

Supplementary Fig. 4 presents the full range mass spectra obtained with *AROMA*. $C_nH_2^+$ species are observed together with $C_nH^+$ species only for odd n values. The neutral precursors are expected to be $C_nH_2$. For even n, polyynes are the expected structure. For odd n, the situation is more complicated with a competition between cumulenic and polyacetylenic structures[26], which most likely accounts for the fact that we observe both $C_nH^+$ and $C_nH_2^+$ species. Regarding smaller species, detection of $C_2H_2^+$ and $C_3H_3^+$ are notable. Both species are believed to be produced during the LDI analysis from the common $C_3H_2$ precursor. Indeed the latter species has a very high proton affinity[27]. In addition, a major dissociation channel of $C_3H_2^+$ leads to $C_2H_2^+ + C$ [28], which is a favourable production mechanism for $C_2H_2^+$ in the *AROMA* conditions, whereas direct ionization of $C_2H_2$ is not a viable mechanism. Finally, evidence for oxidation was seen with a major peak corresponding to $HC_7O$ and a weak one that could be attributed to $HC_5O$. It should be noted that these two stable species nor any other $HC_nO$ species have been detected in the ISM[29,30]. These were the only oxidized species that were detected and it is likely that they were formed by reaction of the deposited molecular precursors with environmental oxygen.

Supplementary Figure 4 shows that low masses, like $C_2H_2$, are more importantly detected for the case of low $H_2$ density. However, this quantification shall not be considered as they correspond to volatile species that remain included in the clusters and their total abundance may change from one sample to another.

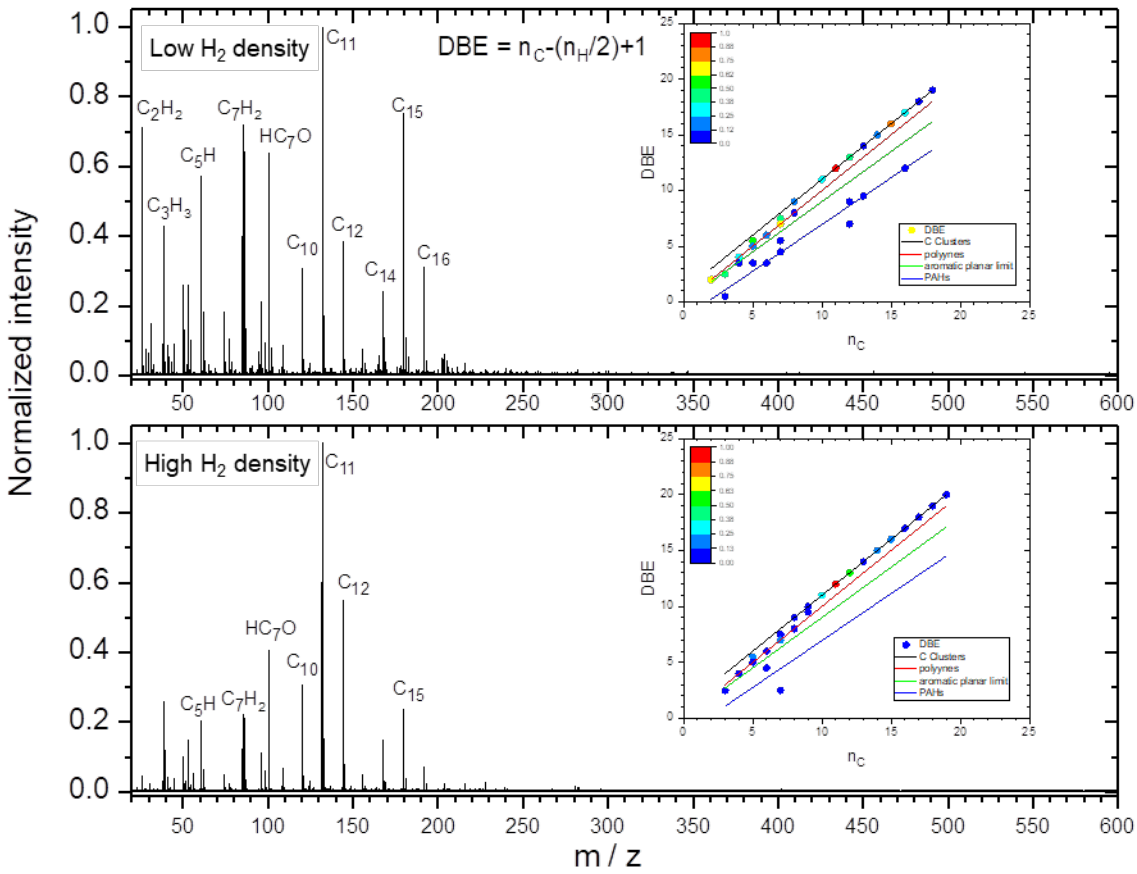


**Supplementary Figure 4.** Full range mass spectra obtained with *AROMA* for *Stardust* samples at low and high $H_2$ densities. The mass peaks are assigned to a chemical formula corresponding to neutral species. Although the laser technique used in *AROMA* minimizes fragmentation compared, for instance, to electron bombardment in a QMS, one should note that fragments of the neutral precursors can be present. Mass peaks corresponding to C clusters and HC clusters were found to dominate the spectra. The distributions of chemical species sizes span from 2 carbon atoms ($C_2H_2$) to a maximum of 19 carbon atoms ($C_{19}$) with the highest peak corresponding to $C_{11}$. The inventory of chemical species looks very similar in both cases, with some variations in the relative peak intensities. The DBE vs carbon number representation (see insets) provides a clearer view of the families of compounds dominating the mass spectra.

The apparent trend of a larger abundance of C clusters relative to HC clusters with the $H_2$ dose must be treated with caution, considering the error-bars. The reported error bars correspond to the relative standard deviation obtained for the total ion signal over a mass range of a family of compounds when the measurement was repeated several times (7 to 10) on natural samples. These error bars, of around 25%, are conservative since they have been derived from a complex matrix.

## 6.- Effect of the temperature in the kinetics models

Apart from the calculations presented in the main text carried out at 500 K, we have performed calculations at other temperatures to evaluate the sensitivity of the calculated abundances to the temperature. We have changed the pressure to use the same density of particles in all calculations and evaluate exclusively the influence of temperature. Supplementary Fig 6 presents an example. At lower temperatures (300 K) the results are qualitatively similar to those obtained at 500 K, with small variation in the peak abundances within the decade. Some masses are slightly higher whereas other decrease. These slight abundance deviations are caused by the dependence of the rate coefficients of the involved reactions in the molecular synthesis. At temperatures higher than 500 K the results gradually modify their trend, with unsaturated hydrocarbons like polyacetylenic chains becoming more abundant at the expense of saturated hydrocarbons, like alkanes. At temperatures above 1000 K the model predicts that the abundance of alkanes should be negligible.

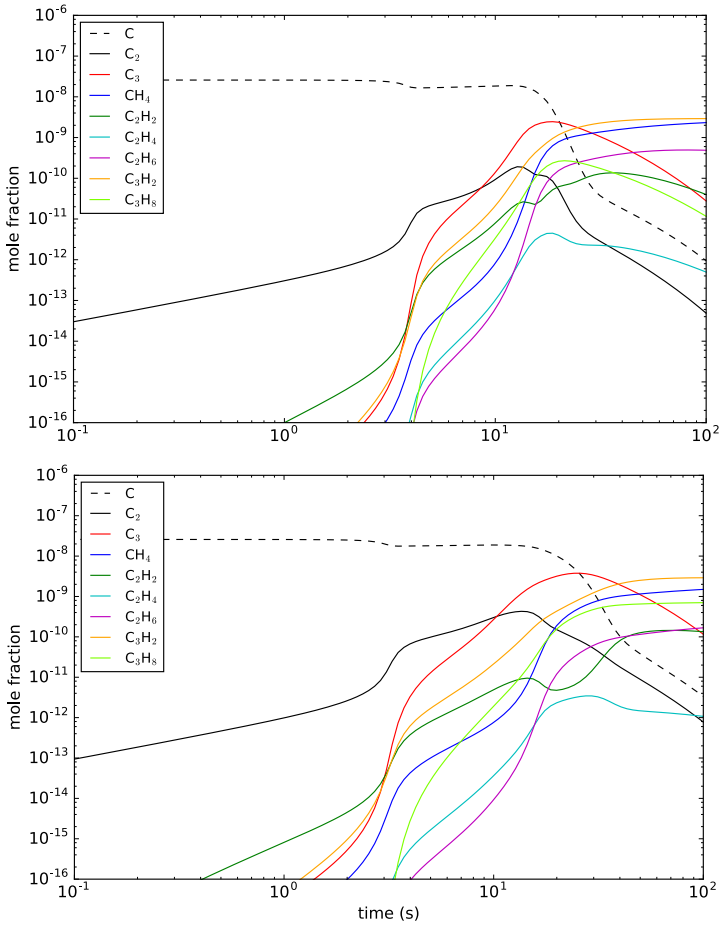


**Supplementary Figure 5. Computed kinetic evolution of the formed species at different temperatures.** Evolution of the chemical composition computed with the chemical kinetics model as the gas flows in the aggregation zone at 500K (upper figure) and 300K (lower figure).

## 7. Thermal Programmed Desorption

In Supplementary Fig. 6 we show a representative TPD experiment. The carbon analogues are deposited in *ANA* module on a Au(111) surface and annealed *in situ* at increasing temperatures. Mass spectrometry is recorded while increasing the temperature. As commented in the main text, consecutive families of small hydrocarbons with increasing carbon number of the family type $C_kH_n$, with 1<k<9 are identified at increasing temperatures (highlighted with blue background). The small hydrocarbons start to desorb from the surface at temperatures as low as 340 K. At higher temperatures, the desorption of small hydrocarbons has occurred and the intensity of the peaks of the associated compounds decreases compared with those obtained at lower temperatures. A good example can be seen in the family $C_3H_n$ which reaches its maximum intensity at a temperature of 433K. At higher temperatures benzene and naphthalene begin to be detected (highlighted with red background).

Importantly the intensity of the associated peak at 78 a.m.u increases with temperature. The increase is monotonous up to the maximum temperature examined of 700K. We also can distinguish mass 91, which can be attributed to toluene fragmentation. These results point towards the processing-induced formation of benzene after thermal processing of the analogues that is possibly mediated by the catalytic activity of the surface. However, we must point out that Au surfaces are notorious for their low-reactivity and low catalytic activity[31]. We have obtained similar results for TPD experiments on other inert substrates such as HOPG and SiOx. Therefore, aromatic formation from thermal processing of the analogues seems to be a robust process. In the real environment of AGB stars other processing mechanisms apart from temperature may be present, such as UV absorption or ionization radiation, which may further promote the conversion of non-aromatics into aromatic molecules and suggest an alternative route for the formation of PAHs.

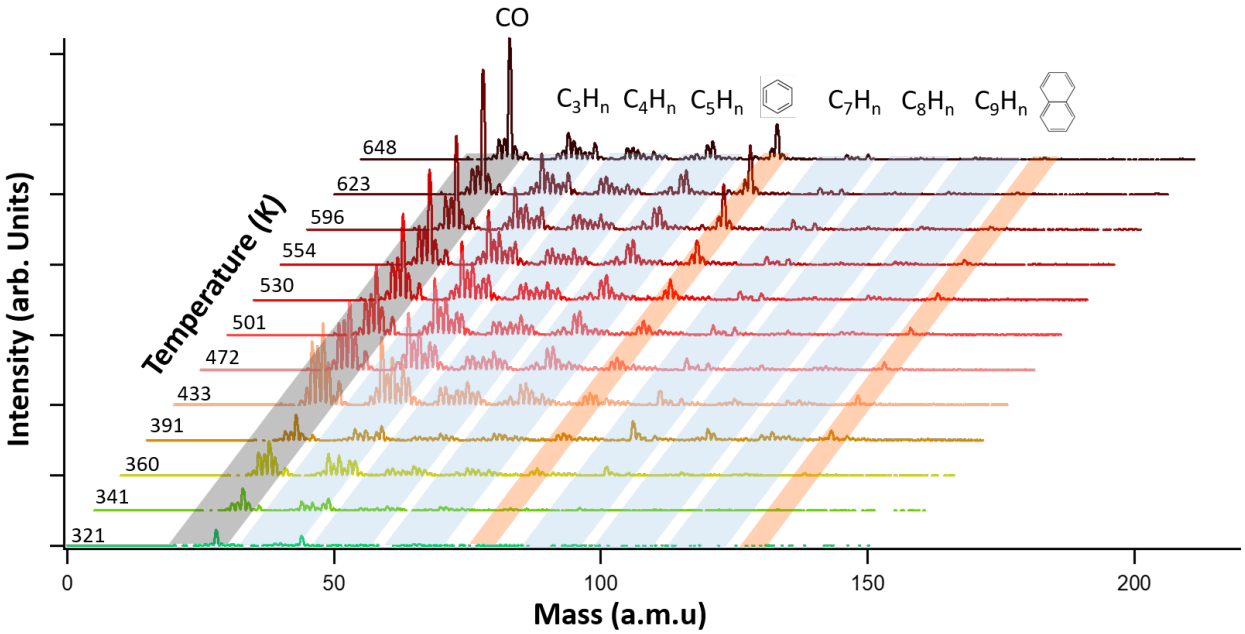


**Supplementary Figure 6. Thermal programmed desorption** of the carbon analogues formed with high hydrogen density deposited on Au(111) annealed at increasing temperatures The temperature at the start of each spectrum is marked on the left-hand side of the figure.. Spectral range from 20 to 150 a.m.u. The spectra are vertically shifted for clarity.